Miscibility and Crystallization Behavior of Poly(3-hydroxybutyrate-*co*-3-hydroxyvalerate)/Poly(vinyl acetate) Blends

Hsiu-Jung Chiu

Department of Chemical and Materials Engineering, Ta Hwa Institute of Technology, Chiunglin, Hsinchu 30703, Taiwan, Republic Of China

Received 30 August 2004; accepted 10 June 2005
DOI 10.1002/app.22823
Published online 12 January 2006 in Wiley InterScience (www.interscience.wiley.com).

ABSTRACT: The miscibility and crystallization behavior of poly(3-hydroxybutyrate-*co*-3-hydroxyvalerate) (P(HB-*co*-HV))/poly(vinyl acetate) (PVAc) blends have been investigated by differential scanning calorimetry (DSC) and polarized optical microscopy (POM). It was found that P(HB-*co*-HV)/PVAc blends were miscible in the melt over the whole compositions. Thus the blend exhibited a single glass transition temperature (T_g), which increased with increasing PVAc composition. The spherulitic morphologies of P(HB-*co*-HV)/PVAc blends indicated that the PVAc was predominantly segregated into P(HB-*co*-HV) interlamellar or interfibrillar regions during P(HB-*co*-HV) crystallization because of the volume-filled spherulites. As to the crystallization kinetics study, it was found that the overall crystallization and crystal growth rates decreased with the addition of PVAc. The kinetics retardation was primarily attributed to the reduction of chain mobility and dilution of P(HB-*co*-HV) upon mixing with higher T_g PVAc. The overall crystallization rate was predominantly governed by the spherulitic growth rate and promoted by the samples treated with the quenched state because of the higher nucleation density.
 J Appl Polym Sci 100: 980–988, 2006

Key words: miscibility; poly(3-hydroxybutyrate-*co*-3-hydroxyvalerate); glass transition temperature; crystallization kinetics

INTRODUCTION

Crystallization kinetics of melt-miscible blends of crystalline and amorphous polymers has been extensively studied.[1–15] When crystallization occurs below the melting point of the crystalline component, the process involves two types of polymer transport, namely diffusion of the crystallizable component toward the crystal growth front and a simultaneous rejection of the amorphous component. This crystallization process produces a liquid–solid phase separation, leading to a variety of morphological patterns closely governed by the kinetics of the two types of polymer transport. In this case, the morphological formation may be kinetically controlled by the thermal history and composition to achieve tailor-made properties for the blends. Therefore, investigation of the crystallization kinetics of polymer blends containing crystallizable components also has practical significance.

Correspondence to: H.-J. Chiu (hjc@thit.edu.tw).
Contract grant sponsor: National Science Council, Republic of China; contract grant number: NSC 92–2216-E-233–001.

Bacterially synthesized poly(3-hydroxybutyrate) (PHB) and its copolymer with 3-hydroxyvalerate (i.e., P(HB-*co*-HV)) with biodegradability and biocompatibility characteristics are crystalline polymers. They are attractive for environmental waste management when used in specific applications. They are naturally occurring and harmlessly biodegradable to water and carbon dioxide by a wide variety of bacteria.[16–18] PHB has some disadvantages such as high brittleness, poor processability, and poor thermal stability, which can be promoted by the PHB crystallization process kinetically. Blending with other polymers or copolymerization with various monomer units is an efficient route to affect the crystallization of PHB to tailor the desired properties. The melt-miscible blends with PHB have extensively investigated such as PHB/poly(epichlorohydrin) (PECH),[1,2] PHB/poly(vinyl acetate) (PVAc),[3–5] and PHB/atactic-PHB,[6,7] PHB/poly(vinyl phenol) (PVPh)[8,9] blends. The P(HB-*co*-HV) is one of the most important copolymers of PHB family, which were isolated from *Alcaligenes eutrophus* grown in culture media containing propionic acid and glucose, and have been developed by Imperical Chemical Ind.[19] Comparing with blends containing PHB, the melt-miscible blends containing P(HB-*co*-HV) has less attention. As studied previously, we have reported the miscibility, crystallization kinetics, and lamellar morphology of P(HB-*co*-HV)/PMMA blends.[20,21] In this study, we

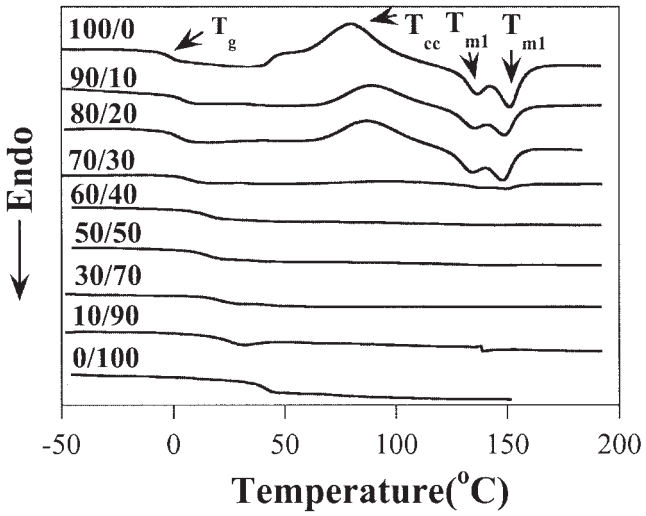

Figure 1 DSC heating scans showing glass transition temperature (T_g) followed by the cold crystallization (T_{cc}) and two melting points (T_{m1} and T_{m2}).

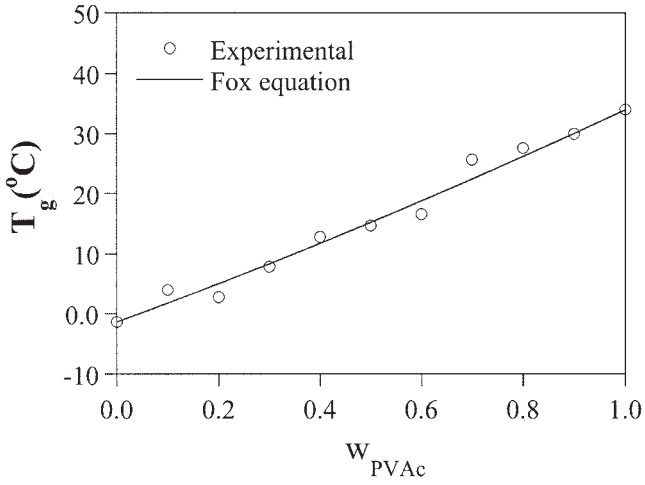

Figure 2 T_g composition dependence of P(HB-*co*-HV)/PVAc blends.

present our results obtained on the phase behavior and crystallization kinetics for the blends of P(HB-*co*-HV) and PVAc. It is shown that this system also exhibits miscibility. Further, it is demonstrated that the addition of PVAc to P(HB-*co*-HV) results in a decrease in both the spherulitic growth rate and the overall crystallization rate.

EXPERIMENTAL

Materials and samples preparation

P(HB-*co*-HV) ($M_n = 1.41 \times 10^5$ and $M_w = 2.13 \times 10^5$) copolymer containing 10 mol % HV content, and PVAc ($M_w = 8.3 \times 10^4$) were purchased from Fluka Chemical Co. and Aldrich, respectively. P(HB-*co*-HV) was blended with PVAc by weight and using *N*,*N*-dimethyl formide (DMF) as solution casting. The blending components were dissolved in DMF at room temperature, yielding a 1 wt % solution. The solution was subsequently poured onto a Petri dish and the blend film was obtained after evaporating most of the solvent on a hot plate at ~90°C. The blend film was further dried in a vacuum oven at 50°C for at least 24 h till constant sample weight. TGA measurement of the dried films showed negligible weight loss above the boiling point of DMF, indicating nearly complete removal of solvent for the blend films.

Polarized optical microscopy

The spherulitic morphology and growth rate were monitored with a Zeiss polarized optical microscope. The sample was first melted on a Linkam HFS91 hot stage at 190°C for 1 min to eliminate the previous thermal history, and then quickly transferred to another hot stage equilibrated at the desired crystallization temperature (T_c), where spherulitic growth was monitored. Micrographs were taken at intervals for

TABLE I
Values of Glass Transition Temperature (T_g), Cold Crystallization Temperature (T_{cc}), and Two Melting Point Temperatures (T_{m1} and T_{m2}) of P(HB-*co*-HV)/PVAc

Composition of P(HB-*co*-HV)/PVAc	Experimental T_g (°C)	Fox equation T_g (°C)	T_{cc} (°C)	T_{m1} (°C)	T_{m2} (°C)
100/0	−1.37	−1.37	79.25	136.79	150.94
90/10	3.96	1.80	87.73	135.85	149.06
80/20	2.76	5.04	87.75	134.91	148.11
70/30	7.81	8.36	–	–	–
60/40	12.80	11.75	–	–	–
50/50	14.69	15.23	–	–	–
40/60	16.56	18.80	–	–	–
30/70	25.64	22.46	–	–	–
20/80	27.58	26.21	–	–	–
10/90	29.97	30.05	–	–	–
0/100	34.00	34.00	–	–	–

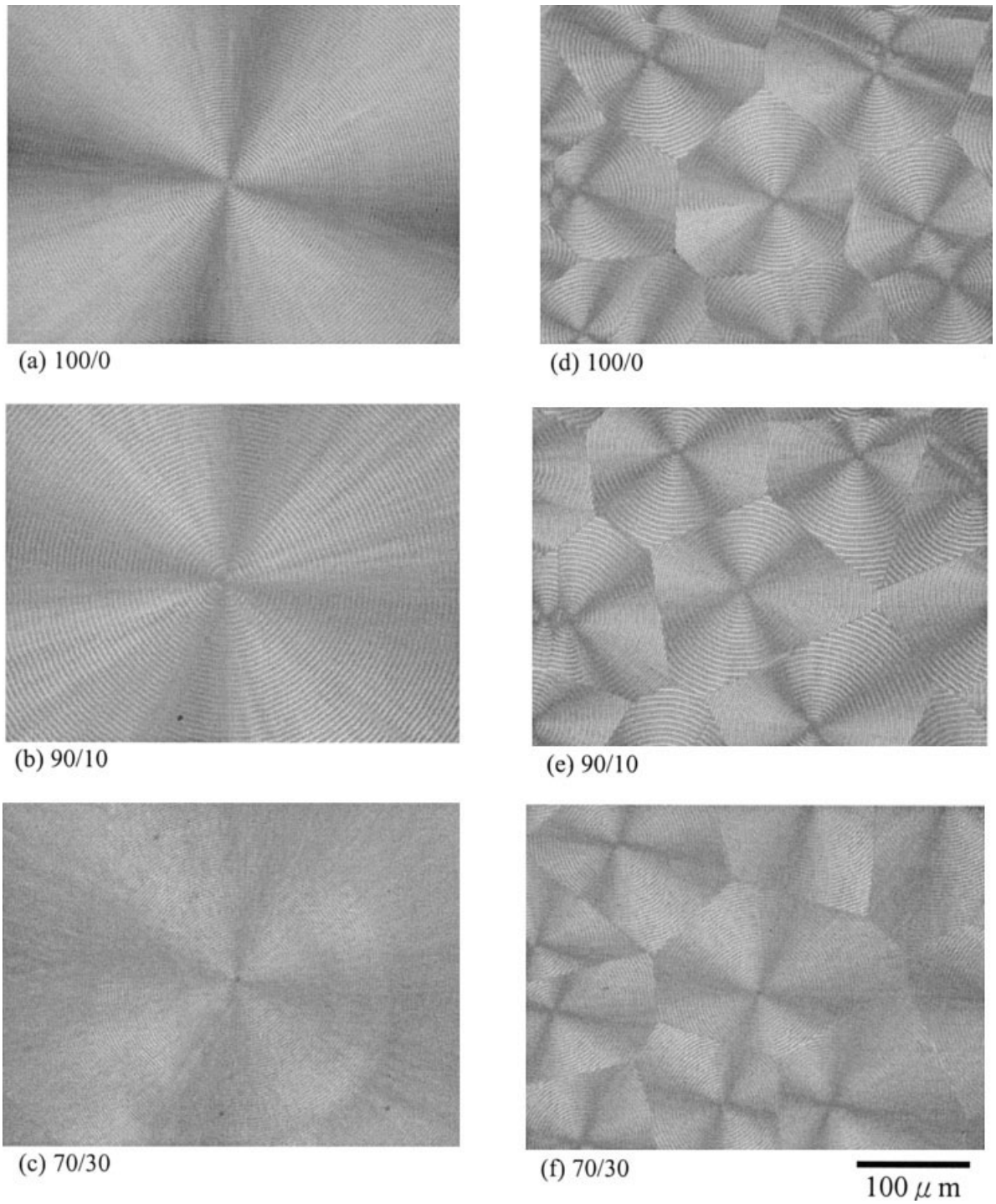

Figure 3 Spherulitic morphologies of P(HB-*co*-HV)/PVAc blends crystallized at T_c = 70°C Samples transferred from the melt state prior to crystallization (a,b,c); samples transferred from the quenched state prior to crystallization (d,e,f).

measuring the spherulite radii (R) at various time periods. The growth rate was calculated from the change of spherulitic radius with time, dR/dt.

Differential scanning calorimetry

Differential scanning calorimetry (DSC) was performed with a TA instrument 2000 DSC, which was calibrated with Indium prior to use. The sample was heated to 190°C for 1 min, and then quickly quenched to −50°C with liquid nitrogen. Subsequently, the glass transition temperature (T_g), cold crystallization temperature (T_{cc}), and melting point temperature (T_m) were measured by reheating the sample from −50°C to 190°C at a heating rate of 20°C/min. For the overall crystallization experiment, sample prior to crystalliza-

tion has been proceeded by two different types: the melt and quenched states, respectively. For the melt state, the sample was first melted on a Linkam HFS91 hot stage at 190°C for 1 min, and then rapidly transferred into DSC equilibrated at T_c = 40°C to allow crystallization. For the quenched state, the blends were directly quenched from the melt state with liquid N_2 for 3 min, then rapidly transferred into DSC equilibrated at T_c = 40°C to allow crystallization. The isothermal crystallization exotherm and the temporal development of crystallization exotherm were recorded; these data would later be analyzed according to the usual procedure of evaluating the relative degree of crystallinity, $X(t)$

$$X(t) = \frac{\int_0^t \left(\frac{dH}{dt}\right) dt}{\int_0^x \left(\frac{dH}{dt}\right) dt} \quad (1)$$

where the numerator represents the area of isotherms accumulated as of time t and the denominator is the total exotherm area.

RESULTS AND DISCUSSION

Glass transition temperature

In general, the miscibility of polymer blends can be determined by thermal characterization. Miscibility of blends containing two amorphous polymers is detected by the presence of a single glass transition temperature (T_g) intermediate between those of the two component polymers. For ideal systems, which are miscible and amorphous over the entire composition range, the T_g composition dependence of the blend can be predicted by Fox equation.[22] Figure 1 shows DSC heating scans showing the T_g followed by cold crystallization temperature (T_{cc}) and two melting point temperatures (T_{m1} and T_{m2}). The peaks of T_{cc}, T_{m1}, and T_{m2} can clearly be observed as composition contained PVAc of <30 wt %. Table I indicates the data of relating T_g, T_{cc}, T_{m1}, and T_{m2}. The T_gs of neat P(HB-*co*-HV) and PVAc were −1.2°C and 34°C, respectively. The blends exhibited a single T_g intermediate between those of the two blended polymers. The T_g value increased with increase in w_{PVAc}. This means that the P(HB-*co*-HV)/PVAc blends were completely miscible in the melt over the whole compositions. The observed T_g on weight fraction of PVAc (w_{PVAc}) was shown in Figure 2 again. The T_g composition relation can be expressed well by the theoretical Fox equation[22]

$$\frac{1}{T_{g,\text{blend}}} = \frac{w_{\text{P(HB-}co\text{-HV)}}}{T_{g,\text{P(HB-}co\text{-HV)}}} + \frac{w_{\text{PVAc}}}{T_{g,\text{PVAc}}} \quad (2)$$

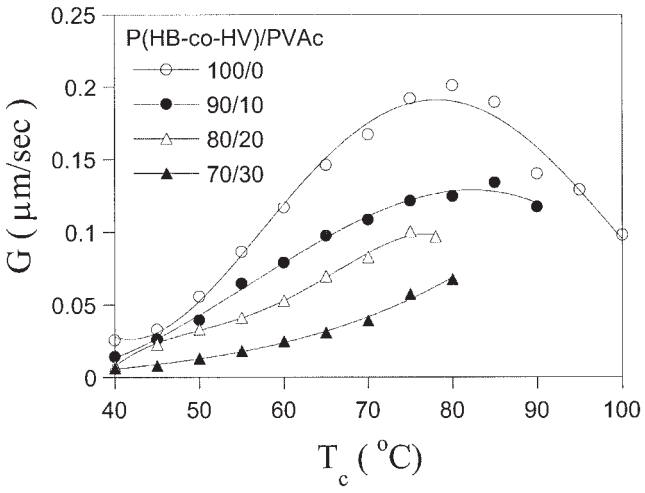

Figure 4 Variation of the spherulitic growth rate as a function of crystallization temperature.

where $T_{g,\text{blend}}$, $T_{g,\text{P(HB-}co\text{-HV)}}$, and $T_{g,\text{PVAc}}$ are T_gs of blend, P(HB-*co*-HV), and PVAc, respectively, and $w_{\text{P(HB-}co\text{-HV)}}$ and w_{PVAc} are the weight fractions of P(HB-*co*-HV) and PVAc. From the Fox equation, it was noticed that the measured T_g was in good agreement with the calculated T_g. This implies that the intermolecular interaction between P(HB-*co*-HV) and PVAc was not strong.

The miscibility in blends containing a crystalline polymer could be further characterized by the crystallization behavior of the crystalline polymer. In the present study, in addition to the T_g method, the T_{cc} of quenched samples on the same DSC heating scans (at second heating run) as shown in Figure 1 and Table I can be used together to identify the miscibility of the P(HB-*co*-HV)/PVAc blends. It is known that T_{cc} must occur at a temperature above the T_g where the crystallizable polymer chains possess enough segmental mobility to crystallize, indicating that the lower T_g with larger molecular mobility should be accompanied by the lower T_{cc}, inversely, the higher T_g must has higher T_{cc}. It can be observed in Figure 1 and Table I that not only the exotherm decreased but also the T_{cc} shifted toward higher temperature with the addition of PVAc up to 20 wt % and the dependence hardly noticeable when compositions were >30 wt % PVAc, indicating that the crystallization process took place from a single homogeneous phase and the presence of PVAc actually hindered the crystallization of P(HB-*co*-HV) in blends. This result further supports that the P(HB-*co*-HV)/PVAc blends were miscible in the melt.

On the other hand, the multiple melting points (T_{m1} and T_{m2}) were also observed in Figure 1. Such a multiple melting behavior may be associated with the occurrence of melting, recrystallization, and remelting in the melting region. The measured T_g was in good agreement with the calculated T_g by Fox equation, as

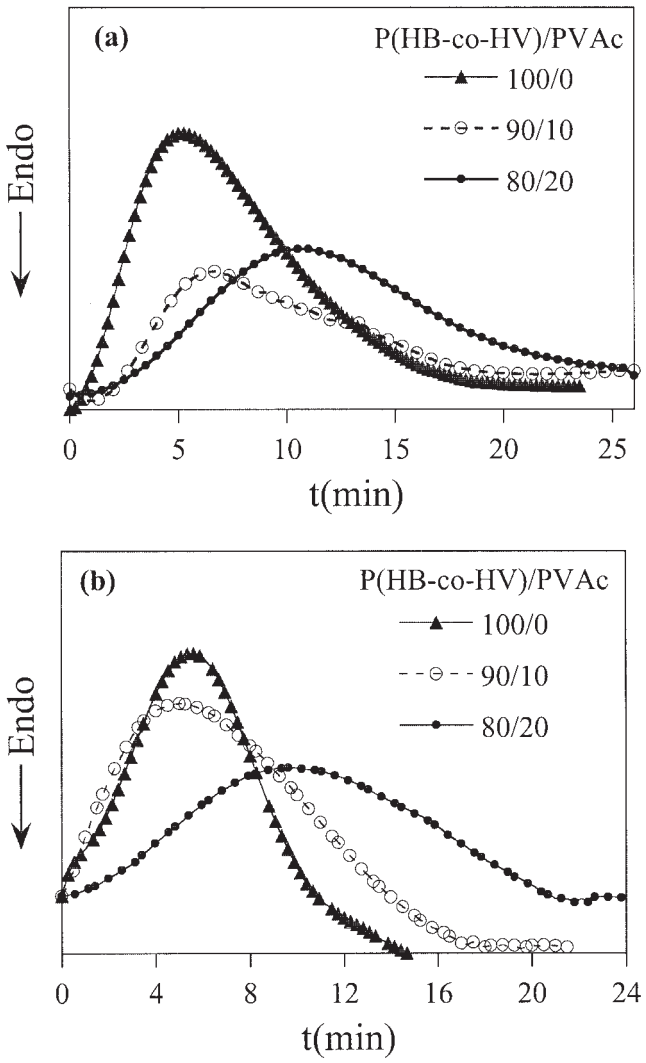

Figure 5 Crystallization exotherm of P(HB-*co*-HV)/PVAc blends crystallized at T_c = 40°C. (a) Sample transferred from the melt state prior to crystallization; (b) Sample transferred from the quenched state prior to crystallization.

shown in Figure 2 and Table I, implying that the composition of blends in the quenched (amorphous) state did not deviate from the initial composition of sample prepared. Therefore, it was suggested that the T_{m1} is mainly the melting behavior of the crystals, as formed at T_{cc}, while the T_{m2} represents the following melt-recystallization crystals.

Spherulitic morphology

The spherulitic morphology of crystalline polymers can be observed conveniently by polarized optical microscopy (POM). Figure 3 displays the spherulitic structures of P(HB-*co*-HV)/PVAc blends crystallized at T_c = 70°C, where the samples were transferred from the melt state and quenched state prior to crystallization, respectively. Irrespective of the sample treatment procedure, no apparent evidence of liquid–liquid phase separation was observed up to impingement of the spherulitic structures. The major blends that were studied exhibited a banded Maltese-cross spherulitic structure as neat PHB.[5,16] The phenomenon of the banded spherulitic structure is always observed on the crystalline polymer or its blends such as PHB/PEO[23] and PVDF/PBA[24] systems, which was believed to arise from the cooperative twisting of radiating lamellar crystals because of the fast crystallization. Since the spherulitites were volume-filling textures, this basically indicates the intraspherulitic segregation of PVAc. In other words, the amorphous PVAc was segregated into the interlamellar or interfibrillar regions during the crystallization of P(HB-*co*-HV). The nucleation of samples treated by the quenched (glassy) state in Figures 3(d)–3(f) is obviously higher than that from the melt state in Figures 3(a)–3(c). This was suggested that when the sample was transferred from the

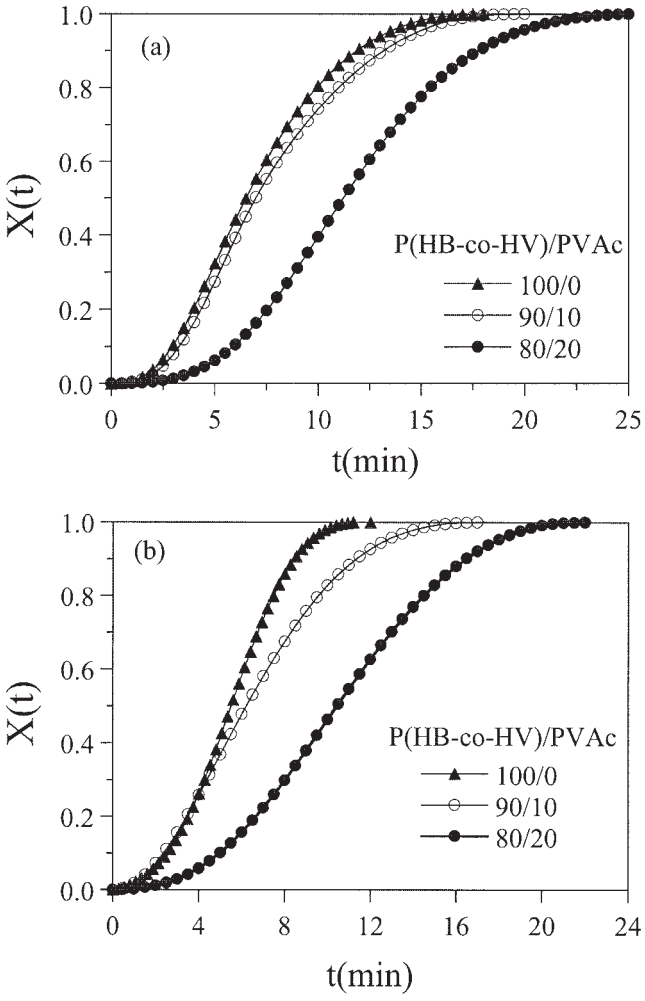

Figure 6 Temporal development of $X(t)$ of P(HB-*co*-HV)/PVAc blends crystallized at T_c = 40°C. (a) Sample transferred from the melt state prior to crystallization; (b) Sample transferred from the quenched state prior to crystallization.

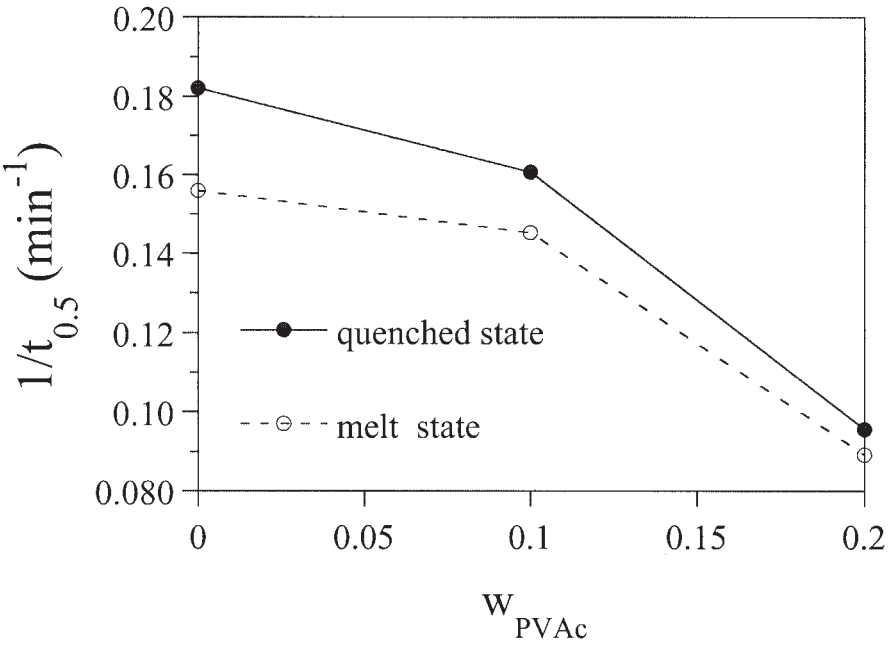

Figure 7 Variation of $1/t_{0.5}$ as a function of PVAc composition.

quenched state prior to crystallization, the temporarily frozen molecular chains might offer an opportunity for heterogeneous nucleation and depress the mobility of molecules during the crystallization process, leading to a slow growth and fast nucleation rates. The fast nucleation and slow growth rates could induce the formation of small spherulites after impingement and thus produced the higher nucleation density.

Spherulitic growth

The spherulitic radial growth rates (G) of neat P(HB-*co*-HV) and P(HB-*co*-HV)/PVAc blends were determined by measuring the spherulitic radii R at various time periods during isothermal crystallization. For each composition studied, R was observed to increase linearly with time up to the point of impingement, indicating a constant growth rate throughout the crystallization process. The linearity of R implies that the PVAc component, which is segregated away from crystal growth front, does not accumulate at the spherulitic growth front, but should be trapped within the interlamellar or interfibrillar regions in the growing spherulites. Figure 4 depicts the variation of spherulite growth rate (G) with increasing T_c at each blend composition. It was observed that G decreased remarkably with increase in PVAc composition at a given T_c. Such a marked reduction in growth rate has been widely observed in blends[25–27] with an amorphous polymer with a higher T_g, which has been attributed to the decrease of molecular mobility and the dilution of the crystalline component. The depression of equilibrium melting point (T_m^0) due to segmental miscibility may also contribute to the reduction of crystallization kinetics in miscible polymer blends, but this effect is usually less significant for a system with relatively weak interactions. Similarly, the same reason may be used to explain the growth rate depression in the P(HB-*co*-HV)/PVAc system. A decrease in G with the addition of higher T_g PVAc component also supports that the P(HB-*co*-HV)/PVAc blends were miscible in the melt.

On the other hand, the trend of curves in Figure 4 shows the maximum of G in the neighborhood of 80°C at each composition. It is well known that the crystallization window of a crystalline polymer must lie between T_g and T_m^0. When the desired T_cs locate toward T_g, the crystallization kinetics would be controlled by the chain mobility such that the rate increases with increase in T_c in this mobility regime. In contrast, if the desired T_cs are located toward T_m^0, the crystallization rate would be controlled by the thermodynamic driving force of crystallization (the thermodynamically controlled regime). The interplay between these two factors produces a maximum in crystallization rate at T_c^{max} between T_g and T_m^0. It is observed that the T_c^{max}s of neat P(HB-*co*-HV) and P(HB-*co*-HV)/PVAc blends were in the neighborhood of 80°C. Such a consequence is similar to the result in the P(HB-*co*-HV)/PMMA[20] system as previously studied in our laboratory.

Overall crystallization kinetics

It is well known that the overall crystallization rate is determined by both the nucleation and growth rates.

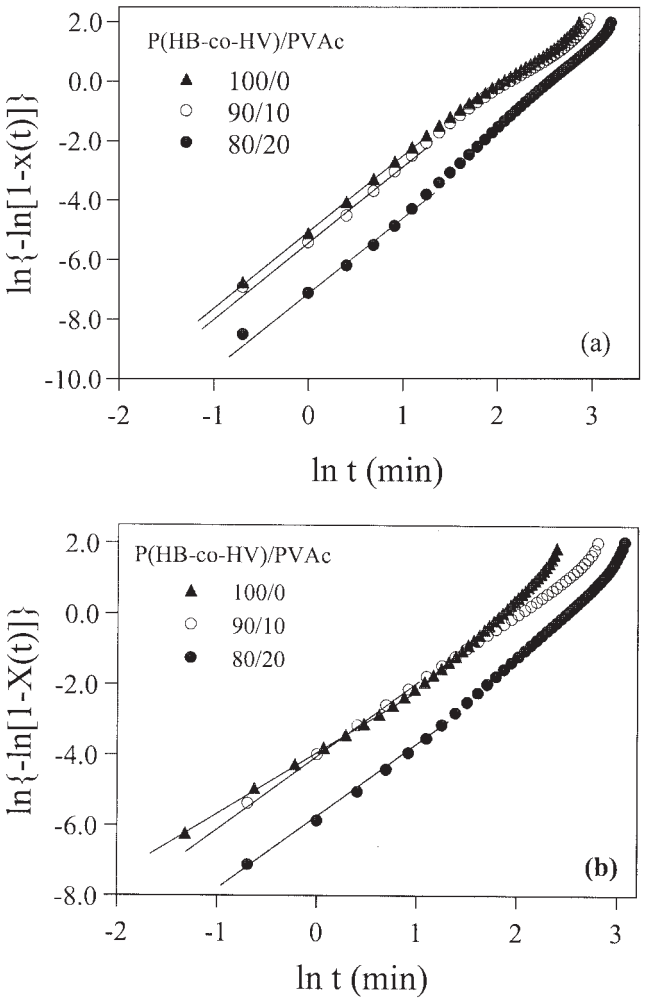

Figure 8 Plot of the Avrami equation for P(HB-*co*-HV)/PVAc blends at crystallized T_c = 40°C. (a) Sample transferred from the melt state prior to crystallization; (b) Sample transferred from the quenched state prior to crystallization.

In the present study, the influences of composition and sample treatment on the overall crystallization rate have been investigated. Figure 5 displays the crystallization exotherm dependence on crystallization time. It was observed that the exothermic peak shifted to larger amount of time and the height in the peak depressed with increase in PVAc. For 70/30 composition, the exothermic peak was not observed because of extremely slow crystallization so that the exotherm could not be observed. Therefore, we primarily focused on the crystallization kinetics of the composition with no more than 20 wt % PVAc. Figure 6 shows the temporal development of $X(t)$ of each blend composition. It can be seen that the crystallization isotherms displayed the characteristic sigmoidal shape. Furthermore, the initial slope of the isotherms decreased with increase in PVAc, indicating a progressively slower crystallization rate. This means that the presence of PVAc would strongly retard the overall crystallization kinetics of P(HB-*co*-HV). The half-time of crystallization ($t_{0.5}$), defined as the time required to attain half of the final crystallinity, was evaluated from these curves. The overall crystallization rate can be represented by $1/t_{0.5}$. Figure 7 displays the dependence of $1/t_{0.5}$ on composition. It was clearly observed that the overall crystallization rate ($1/t_{0.5}$) decreased with increase in PVAc, which was primarily attributed to the reduction of molecular mobility of P(HB-*co*-HV) arising from the increase of T_g upon blending with PVAc. On the other hand, the values of $1/t_{0.5}$ of samples treated by the quenched state were larger than those of samples treated by the melt state. In other words, the overall crystallization rate could be promoted as the samples were transferred from the quenched state because of the higher nucleation density (rate) as previously stated in Figure 3.

To obtain further details concerning the overall crystallization kinetics of neat P(HB-*co*-HV) and P(HB-*co*-HV)/PVAc blends, the kinetics of the overall crystallization of each sample was further analyzed on the basis of the Avrami equation[28–30]

$$\ln \{ -\ln [1 - X(t)]\} = \ln k + n \ln t \qquad (3)$$

where k is the overall crystallization rate constant containing contributions from both nucleation and growth rates, and n is the Avrami exponent, which depends on the nucleation and growth mechanism of the crystals. The plot of $\ln\{-\ln[1-X(t)]\}$ versus $\ln t$ produces a linear line with intercept and slope given by k and n, respectively. Figure 8 displays the Avrami plot of each blend composition. It can be seen that the experimental data closely agree with the Avrami equation at low conversion. Plots at high conversion deviate from the equation because of the occurrence of secondary crystallization. Similar to the values reported for blends,[31,32] all the values of n obtained were between 2–3. Such values of n were suggested to be due to the existence of mixed growth, surface nucleation, and two-step crystallization. However, although all n values of the studied samples were <3, these results may roughly confirm a three-dimensional (spherulitic) growth process initiated by heterogeneous nucleation, which was consistent with the observed spherulitic morphology by POM in Figure 3.

The rate constant k defined in eq. (3) has a unit of min^{-n}. In this study, we modified the rate constant as $k_n = k^{1/n}$ to unify the unit of the rate constant as min^{-1}. Figure 9 depicts the composition dependence of k_n. The trend of k_n was similar to that of $1/t_{0.5}$, as in Figure 7. The values of k_n, decreased with the addition of PVAc, which was also attributed to the reduction of molecular mobility because of the added PVAc with high T_g. In addition, the samples crystallized at T_c = 40°C have larger k_n values from the quenched state than from the melt state, which was attributed to the

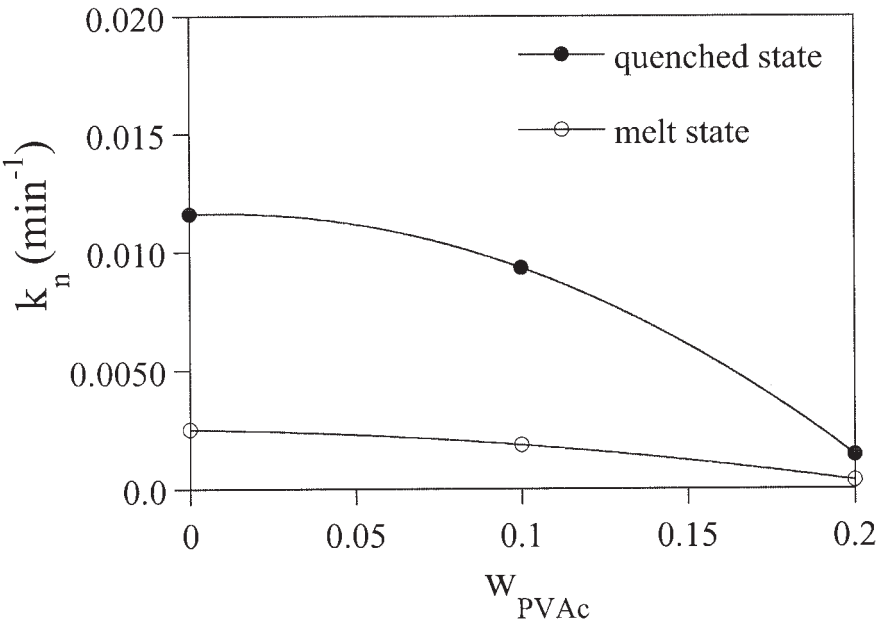

Figure 9 Variation of k_n as a function of PVAc composition.

samples transferred from the quenched state, leading to the higher nucleation density (rate).

According to three-dimensional spherulitic growth, k is defined as

$$k = 4\pi N_\rho (G)^3/3 \quad (4)$$

where N_ρ is the nucleation density corresponding to the number of nuclei per cm^3. From eq. (4) the values of N_ρ are calculated. Figure 10 depicts the composition dependence of log N_ρ. Comparing with neat P(HB-*co*-HV), independent of sample treatment procedure, log N_ρ increased obviously with addition of 10 wt % PVAc, but did not vary to further increase the PVAc content. However, the overall crystallization rate and spherulitic growth rate evidently decrease with increase in PVAc composition, as already stated. This illustrates that the overall crystallization rate was predominantly governed by the spherulitic growth rate. On the other hand, the N_ρ values of samples treated by the quenched state were larger than those of samples treated by the melt state, which was consistent with the observed spherulitic size by POM in Figure 3. This trend could further elucidate that the overall crystallization rate could be promoted by the samples treated with the quenched state because of the higher nucleation density (rate).

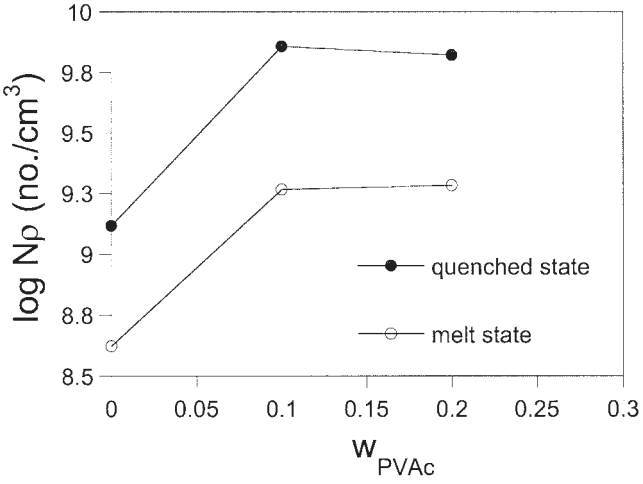

Figure 10 Variation of log $N\rho$ as a function of PVAc composition.

CONCLUSIONS

The miscibility and crystallization kinetics of P(HB-*co*-HV)/PVAc blends have been investigated by DSC and POM. The single glass transition temperatures of the blends within the whole composition range suggest that P(HB-*co*-HV)/PVAc blends were totally miscible in the melt. The spherulitic morphologies of P(HB-*co*-HV)/PVAc blends indicated that PVAc was predominantly segregated into P(HB-*co*-HV) interlamellar or interfibrillar regions during P(HB-*co*-HV) crystallization. The results of a crystallization kinetics study revealed that the overall crystallization and crystal growth rates decreased upon the addition of PVAc. The kinetics retardation was primarily attributed to the reduction of P(HB-*co*-HV) chain mobility and dilution of P(HB-*co*-HV) upon mixing with PVAc. From the results of Avrami analysis, it is inferred that the underlying nucleation mechanism and growth geom-

etry of P(HB-*co*-HV) crystals were not affected by blending. In addition, the overall crystallization rate was predominantly governed by the spherulitic growth rate and could be promoted by the samples treated with the quenched state because of the higher nucleation density.

References

1. Paglia, E. D.; Beltrame, P. L.; Canetti, M.; Seves, A.; Marcandalli, B.; Martuscelli, E. Polymer 1993, 34, 996.
2. Sadocco, P.; Canetti, M.; Seves, A.; Martuscelli, E. Polymer 1993, 34, 3368.
3. Greco, P.; Martuscelli, E. Polymer 1989, 30, 1475.
4. An, Y.; Dong, L.; Xing, P.; Mo, Z.; Zhuang, Y.; Feng, Z. Eur Polym J 1997, 33, 1449.
5. Chiu, H. J.; Chen, H. L.; Lin, T. L.; Lin, J. S. Macromolecules 1999, 32, 4969.
6. Peace, R.; Brown, G. R.; Marchessault, R. H. Polymer 1994, 35, 3984.
7. Abe, H.; Doi, Y.; Satkowski, M. M.; Noda, I. Macromolecules 1994, 27, 50.
8. Iriondo, P.; Iruin, J. J.; Fernandez-Berrodi, M. J. Polymer 1995, 36, 3235.
9. Xing, P.; Dong, L.; An, Y.; Feng, Z.; Avella, M.; Martuscelli, E. Macromolecules 1997, 30, 2726.
10. Chitrangad, B.; Middleman, S. Macromolecules 1981, 14, 352.
11. Liu, A. S.; Liar, W. B.; Chiu, W. Y. Macromolecules 1998, 31, 6593.
12. Martuscelli, E.; Silverstre, C.; Gismondi, C. Makromol Chem 1985, 186, 16.
13. Alfonso, G. C.; Russell, T. P. Macromolecules 1986, 19, 1143.
14. Greveceur, G.; Groeninckx, G. Macromolecules 1991, 24, 1190.
15. Cheung, Y. W.; Stein, R. S. Macromolecules 1994, 27, 2512.
16. Barham, P. J.; Keller, A.; Otun, E. L.; Holmes, P. A. J Mater Sci 1984, 19, 2781.
17. Hocking, P. J.; Marchessault, R. H. In Chemistry and Technology of Biodegradable Polymers; Griffin, G. I. L., Ed.; Blackie Academic & Professional: London, 1994; p 48.
18. Erhoogt, H.; Ramsay, B. A.; Favis, B. D. Polymer 1994, 35, 5155.
19. Holmes, P. A. In Developments in Crystalline Polymers; Bassett, D. C., Ed.; Elsevier: New York, 1988; p 1.
20. Chiu, H. J. J Appl Polym Sci 2004, 92, 3595.
21. Chiu, H. J.; Shu, W. J. J Polym Res, to appear.
22. Fox, T. G. Bull Am Phys Soc 1956, 2, 1123.
23. You, J. W.; Chiu, H. J.; Don, T. M. Polymer 2003, 44, 4355.
24. Penning, J. P.; Manly, R. St. J. Macromolecules 1996, 29, 84.
25. Flory, P. J. J Chem Phys 1949, 17, 223.
26. Mandelkern, L. J Appl Phys 1955, 26, 443.
27. Boon, J.; Azcue, J. M. J Polym Sci Polym Phys Ed 1968, 6, 885.
28. Avrami, M. J. Chem Phys 1939, 7, 1130.
29. Avrami, M. J. Chem Phys 1940, 8, 212.
30. Avrami, M. J. Chem Phys 1941, 9, 177.
31. Hay, J. N.; Sharma, L. Polymer 2000, 41, 5799.
32. Lisowski, M. S.; Liu, Q.; Cho, J.; Runt, J. Macromolecules 2000, 34, 4842.